AGU PUBLICATIONS

Geophysical Research Letters

RESEARCH LETTER
10.1002/2016GL070350

Key Points:
- Atmospheric baroclinic to barotropic conversion is localized at midlatitudes and responsible for the barotropization of the eddy-driven jet
- The supercriticality affects the latitudinal behavior of eddy-eddy interactions
- At high latitudes, eddy-eddy interactions carry the energy up to the Rhines scale and the enstrophy downscale

Supporting Information:
- Supporting Information S1

Correspondence to:
R. Chemke,
rei.chemke@weizmann.ac.il

Citation:
Chemke, R., T. Dror, and Y. Kaspi (2016), Barotropic kinetic energy and enstrophy transfers in the atmosphere, *Geophys. Res. Lett.*, *43*, 7725–7734, doi:10.1002/2016GL070350.

Received 23 MAY 2016
Accepted 8 JUL 2016
Accepted article online 13 JUL 2016
Published online 26 JUL 2016

©2016. American Geophysical Union. All Rights Reserved.

Barotropic kinetic energy and enstrophy transfers in the atmosphere

R. Chemke[1], T. Dror[1], and Y. Kaspi[1]

[1]Department of Earth and Planetary Sciences, Weizmann Institute of Science, Rehovot, Israel

Abstract The midlatitude atmosphere is characterized by turbulent eddies that act to produce a depth-independent (barotropic) mean flow. Using the NCEP (National Centers for Environmental Prediction) Reanalysis 2 data, the latitudinal dependence of barotropic kinetic energy and enstrophy are investigated. Most of the barotropization takes place in the extratropics with a maximum value at midlatitudes, due to the latitudinal variations of the static stability, tropopause height, and sphericity of the planet. Barotropic advection transfers the eddy kinetic energy to the zonal mean flow and thus maintains the barotropic component of the eddy-driven jet. The classic description of geostrophic turbulence exists only at high latitudes, where the quasi-geostrophic flow is supercritical to baroclinic instability; the eddy-eddy interactions carry both the barotropization of eddy kinetic energy upscale to the Rhines scale and the barotropization of eddy potential enstrophy downscale.

1. Introduction

In the atmosphere, large-scale eddies, defined here as departures from zonal mean, play a major role in the meridional distribution of heat and momentum [*Held*, 1975; *Held and Hoskins*, 1985; *Schneider*, 2006]. These eddies are mostly generated by baroclinic instability at midlatitudes, and decay barotropically, where they transfer barotropic kinetic energy to the zonal mean flow [*Simmons and Hoskins*, 1978; *Lee and Kim*, 2003]. This sustains the more barotropic nature of the eddy-driven jet at midlatitudes, in contrast to the more baroclinic nature of the subtropical jet [*Vallis*, 2006]. Studying the barotropization of the flow is thus essential for fully understanding midlatitude dynamics.

Even though the eddies affect the vertical structure of the flow via the stretching of potential vorticity (PV) [*Charney and Stern*, 1962; *Edmon et al.*, 1980], the quasi-geostrophic (QG) flow has many similar properties to those in two-dimensional turbulence [*Charney*, 1971]. The −3 slope, associated with the forward enstrophy cascade, was indeed documented in atmospheric models [*Koshyk et al.*, 1999; *Koshyk and Hamilton*, 2001; *Hamilton et al.*, 2008], observations [*Nastrom and Gage*, 1985], and reanalysis data [*Boer and Shepherd*, 1983; *Shepherd*, 1987; *Straus and Ditlevsen*, 1999; *Burgess et al.*, 2013]. These reanalysis studies also documented the inverse energy cascade but with no evidence for its associated $-5/3$ slope at large scales.

In the atmosphere, the energy and enstrophy transfers among different scales are more complicated than in a two-dimensional fluid, as they include interactions with vertical wave numbers as well. The first to propose an energy cycle that considers both the vertical and horizontal structures in a two-dimensional turbulence framework were *Rhines* [1977] and *Salmon* [1978]. Using a two-layer QG model, the Rhines-Salmon phenomenology describes the transfers of energy and enstrophy from the baroclinic (deviation from vertical average) to the barotropic mode. They suggest that these transfers occur at the scale of the Rossby deformation radius, where eddy kinetic energy (EKE) is produced by baroclinic instability [*Eady*, 1949]. In the barotropic mode, the fluid behaves as a two-dimensional fluid, with a forward enstrophy and inverse energy cascades. Due to the β effect, the inverse energy cascade is halted at the Rhines scale [*Rhines*, 1975], which separates the Rossby wave and turbulent regimes. The eddy-eddy interactions are thus more prominent as the ratio of the Rhines scale and Rossby deformation radius, which corresponds to the QG supercriticality [*Held and Larichev*, 1996], exceeds unity [*Chemke and Kaspi*, 2015].

Even though the Rhines-Salmon phenomenology was developed in a QG framework using a two-layer model with constant Coriolis and static stability parameters, a large portion of the phenomenology was shown to occur in QG-stratified models [*Smith and Vallis*, 2001, 2002; *Venaille et al.*, 2012], idealized general circulation

models (GCMs) [*Chemke and Kaspi*, 2015], and ocean state estimates [*Chemke and Kaspi*, 2016a]. Nonetheless, several deviations from the phenomenology were also found in a more realistic framework: (i) the energy-containing scale [e.g., *Danilov and Gurarie*, 2002; *Thompson and Young*, 2007], as well as the strength of the energy cycle [e.g., *Arbic and Flierl*, 2004; *Smith and Vallis*, 2002; *Treguier and Hua*, 1988], was shown to depend on bottom drag and topography. (ii) Using both satellite data [*Scott and Wang*, 2005] and models [*Schlösser and Eden*, 2007; *Scott and Arbic*, 2007], the first baroclinic mode in the ocean did not reveal a forward energy cascade as expected from the Rhines-Salmon phenomenology but rather an inverse energy cascade from the Rossby deformation radius to larger scales. (iii) The scale of baroclinic-barotropic EKE transfer was not found to follow the Rossby deformation radius [*Larichev and Held*, 1995; *Chemke and Kaspi*, 2015, 2016a, 2016b]. (iv) The strength and direction of the baroclinic-barotropic energy cycle were shown to depend on latitude in both idealized GCMs [*Chemke and Kaspi*, 2015] and oceanic state estimates [*Chemke and Kaspi*, 2016a].

In this study, the spectral properties of the atmospheric barotropic mode are investigated for the first time as a function of latitude using reanalysis data. This is different than previous studies, which investigated the global spectral behavior of the atmosphere at different pressure levels [*Boer and Shepherd*, 1983; *Shepherd*, 1987; *Trenberth and Solomon*, 1993; *Burgess et al.*, 2013] or observed the vertical average eddy fields [*Straus and Ditlevsen*, 1999]. The reanalysis data enable studying the barotropic mode in a more realistic framework than previous idealized studies, as it provides the best available realization of the observed atmospheric dynamics. An investigation of the oceanic barotropic mode was recently conducted using the ECCO2 state estimate [*Chemke and Kaspi*, 2016a], which showed similar findings to the presented atmospheric results and thus further strengthens the theoretical arguments.

2. Methodology

The latitudinal structure of the barotropic EKE and eddy potential enstrophy in the atmosphere is studied over 37 years (1979–2015) using the National Centers for Environmental Prediction (NCEP) Reanalysis 2 data [*Kanamitsu et al.*, 2002]. This state-of-the-art analysis constrains the T62 NCEP global spectral model with raw-insondes, satellite, and surface marine and land data to produce winds, geopotential height, and temperature at 17 vertical pressure levels with 6 h temporal and 2.5° × 2.5° horizontal resolutions. This resolution is sufficient to capture the behavior of the zonal energy-containing scale and to observe the spectral properties of geostrophic turbulence in the barotropic mode down to where the spectrum rapidly declines into the dissipation range. Repeating this analysis using the ECMWF Reanalysis (ERA-Interim) data [*Dee et al.*, 2011], produces similar findings.

The barotropic EKE and eddy potential enstrophy (Z) zonal spectra are, respectively, calculated around each latitude circle [*Saltzman*, 1957] as

$$\mathrm{bEKE}_k = \left\langle \left|[u]'_k\right|^2 + \left|[v]'_k\right|^2 \right\rangle \tag{1}$$

and

$$\mathrm{b}Z_k = \left\langle \left|[q]'_k\right|^2 \right\rangle, \tag{2}$$

where angle and squared brackets denote a time mean and vertical average, respectively, primes represent deviation from zonal mean, and k is the zonal wave number with a corresponding wavelength,

$$\lambda = \frac{2\pi a \cos(\vartheta)}{k}, \tag{3}$$

where ϑ is latitude and a is Earth's radius. u and v are the zonal and meridional velocities, respectively, and $q = \zeta + f + \frac{\partial}{\partial p}\left(\frac{f_0^2}{S^2}\frac{\partial \psi}{\partial p}\right)$ is the QG potential vorticity (QGPV) [*Charney and Stern*, 1962] in pressure coordinates (p), where ζ is relative vorticity, f is the Coriolis parameter, f_0 is a constant midlatitude value of f, $\psi = \frac{\phi}{f}$ is the stream function, where ϕ is the geopotential, and $S^2 = -\frac{1}{\rho\theta^+}\frac{\partial \tilde{\theta}}{\partial p}$, where ρ is density, $\tilde{\theta}$ is a reference profile of the potential temperature, and θ^+ is the deviation from that reference profile [*Hoskins et al.*, 1985; *Vallis*, 2006]. For studying the spectral behavior of the zonal barotropic EKE, three terms of its tendency equation are computed:

$$CT = -\mathrm{Re}\left\langle [\mathbf{u_h}]'^{*}_k \cdot \left[\mathbf{u}^+ \cdot \boldsymbol{\nabla}\mathbf{u}^+_\mathbf{h}\right]'_k \right\rangle \tag{4}$$

denotes the baroclinic to barotropic conversion,

$$EM = -\mathrm{Re}\left\langle [\mathbf{u_h}]_k'^{*} \cdot \left(\overline{[\mathbf{u}]} \cdot \nabla [\mathbf{u_h}]' + [\mathbf{u}]' \cdot \nabla \overline{[\mathbf{u_h}]} \right)_k \right\rangle \tag{5}$$

denotes the eddy-mean flow interactions, and

$$EE = -\mathrm{Re}\left\langle [\mathbf{u_h}]_k'^{*} \cdot \left([\mathbf{u}]' \cdot \nabla [\mathbf{u_h}]' \right)_k \right\rangle \tag{6}$$

denotes the eddy-eddy interactions, where $\mathbf{u_h}$ and $\mathbf{u}$ denote the horizontal 2-D and 3-D velocity vectors, respectively, asterisk denotes a complex conjugate, the plus sign represents departure from vertical average, and bar denotes a zonal mean. A fourth term that denotes the conversion of barotropic eddy potential energy to EKE is less relevant for studying the interactions among different scales (Figure S1 in the supporting information). Similar terms are, respectively, computed for the Z tendency equation:

$$qCT = -\mathrm{Re}\langle [q]_k'^{*} \left[\mathbf{u}^{+} \cdot \boldsymbol{\nabla} q^{+} \right]_k' \rangle, \tag{7}$$

$$qEM = -\mathrm{Re}\left\langle [q]_k'^{*} \left(\overline{[\mathbf{u}]} \cdot \nabla [q]' + [\mathbf{u}]' \cdot \nabla \overline{[q]} \right)_k \right\rangle, \tag{8}$$

and

$$qEE = -\mathrm{Re}\left\langle [q]_k'^{*} \left([\mathbf{u}]' \cdot \nabla [q]' \right)_k \right\rangle. \tag{9}$$

Equations (4)–(9) also include the spherical metric terms as described in *Chemke and Kaspi* [2015]. On one hand, the one-dimensional Fourier analysis allows investigating the meridional structure of the barotropic mode and the important zonal macroturbulent scales. On the other hand, it contains the lateral transport of EKE and Z among different latitudes. These transfers are found to be less important than the transfers calculated in equations (4)–(9) (Figure S2 in the supporting information). In addition, the isotropic nature of small-scale eddies [e.g., *Shepherd*, 1987; *Chemke and Kaspi*, 2016b] may suggest that energy transfers to different energetic zonal wave numbers represent similar transfers in total wave number space.

3. Barotropization of EKE

The main source of EKE in the barotropic mode is the conversion from all baroclinic modes to the barotropic mode (barotropization, Figure 1a). The barotropization of the flow spans the entire extratropics, with a maximum value at midlatitudes. The nonmonotonic behavior of the barotropization with latitude may be explained using *Held and Larichev* [1996] scaling theory, which suggest that the barotropization should increase with the barotropic root-mean-square velocity (U_{RMS}), vertical shear of the zonal wind (u_z) and f, and decrease with increasing stratification ($N^2 = \frac{g}{\theta}\frac{\partial \theta}{\partial z}$, where g is gravity) and tropopause height (H). As some of the parameters are affected by processes in the energy cycle, the understanding of cause and effect is limited. Furthermore, different than modeling studies [e.g., *Held and Larichev*, 1996; *Smith and Vallis*, 2001, 2002; *Thompson and Young*, 2007; *Venaille et al.*, 2012], the reanalysis data cannot provide a systematic investigation of the relative importance of these parameters in affecting the latitudinal behavior of the barotropization. Thus, it is elucidated based on the relations found in these studies. Figure 2 shows the dependence of the mean barotropization on these zonal mean parameters. The mean barotropization in Figure 2 is calculated as the sum of the barotropization through all wave numbers at latitudes where the mean barotropization is larger than 30% of its maximum value. Thus, each circle corresponds to a specific latitude, where blue (red) circles correspond to latitudes poleward (equatorward) of the latitude of maximum mean barotropization and closed (open) circles correspond to the Northern (Southern) Hemisphere.

In the ocean, the EKE is surface intensified and thus limits the baroclinic-barotropic transfer. This was suggested to occur due to strong stratification in both oceanic models [*Smith and Vallis*, 2001; *Fu and Flierl*, 1980] and at low latitudes in state estimate data [*Chemke and Kaspi*, 2016a]. In the atmosphere, since the stratification increases poleward (Figure 2a), an inverse relation with the barotropization (as suggested by *Held and Larichev* [1996]) is found only at high latitudes (blue circles, Figure 2a), which follows $N^{-10.2\pm1.3}$ (the $\pm$ denotes its 95% confidence interval and $R^2 = 0.92$). This suggest that the stratification might only explain the decrease of the barotropization at high latitudes (Figure 1a).

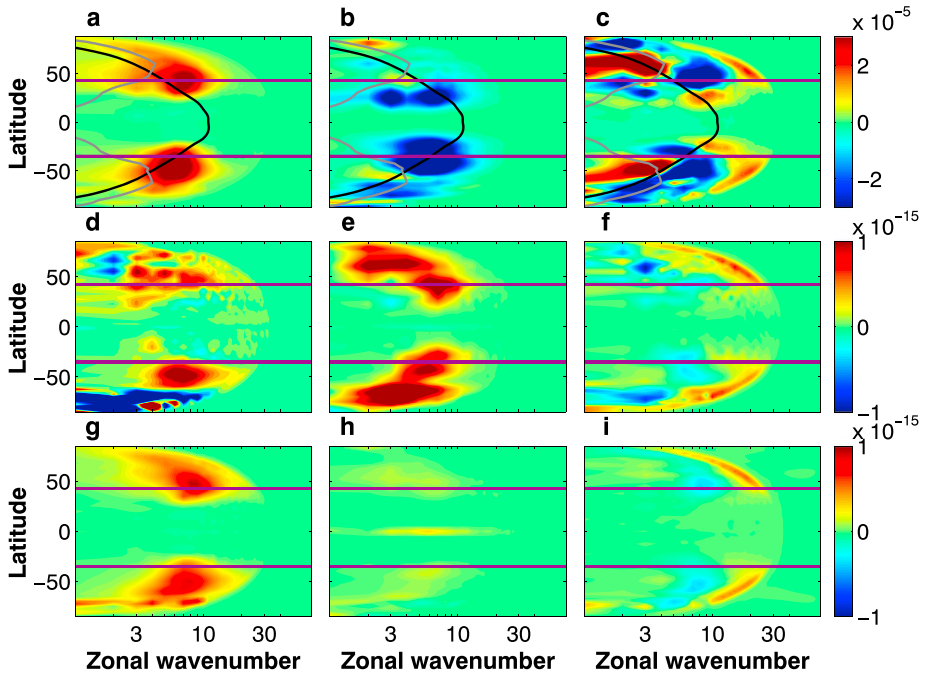

Figure 1. Components of the (a–c) barotropic EKE equation (m^2s^{-3}) and Z equation (s^{-3}) using (d–f) QGPV and (g–i) QGPV with constant f and S^2 as a function of latitude and zonal wave number. Figure 1a shows conversion of baroclinic EKE divided by 5 (equation (4)). Figure 1b shows EKE eddy-mean flow interactions (equation (5)). Figure 1c shows EKE eddy-eddy interactions (equation (6)). Figures 1d and 1g show Z conversion of baroclinic to barotropic (equation (7)). Figures 1e and 1h show Z eddy-mean flow interactions (equation (8)). Figures 1f and 1i show Z eddy-eddy interactions (equation (9)). The gray and black lines in Figures 1a–1c are the Rossby and Rhines wave numbers, respectively. The purple lines are the supercriticality latitude, where the QG supercriticality equals 1. Each component is multiplied by the zonal wave number.

The barotropic EKE, which is used for calculating U_{RMS}, indeed tends to increase the barotropization in both hemispheres (open and closed circles, Figure 2b), but it has low statistical significance and shows stronger dependence in the Northern Hemisphere (NH) ($\propto$ bEKE$^{0.74\pm0.37}$ and $R^2 = 0.48$, closed circles) than in the Southern Hemisphere (SH) ($\propto$ bEKE$^{0.1\pm0.23}$ and $R^2 = 0.05$, open circles). While the vertical shear of the zonal wind barely changes in the SH (open circles, Figure 2c), due to the double jet structure in the extratropics, and at low latitudes in the NH (closed red circles), it tends to increase the barotropization at high latitudes in the NH ($\propto u_z^{1.54\pm0.2}$ and $R^2 = 0.96$, closed blue circles). The large differences between the two hemispheres in the dependence of the barotropization on the barotropic EKE and vertical shear suggest that they are less likely to explain the symmetric behavior of the barotropization in both hemispheres (Figure 1a).

A direct relation between the Coriolis parameter and barotropization occurs only at low latitudes (red circles, Figure 2d) where the barotropization increases and follows $f^{1.86\pm0.27}$ ($R^2 = 0.93$). As the tropopause height decreases with latitude in the extratropics, it presents an inverse relation with the barotropization only at low latitudes (red circles, Figure 2e), which follows $H^{-2.86\pm0.73}$ ($R^2 = 0.82$). Following the World Meteorological Organization definition, the tropopause height is defined as the lowest height where the mean lapse rate is 2 K km^{-1}. The β term (meridional derivative of the Coriolis parameter) affects the barotropization only at high supercriticality, where due to an inverse energy cascade, it enters the energy-containing scale (e.g., the Rhines scale) [*Held and Larichev*, 1996]. The purple lines in Figure 1 (supercriticality latitudes) mark the meridional transition between vertically averaged values of QG supercriticality ($S_c = \frac{f^2 u_z}{\beta H N^2}$, following *Held and Larichev* [1996]) above and below unity. Thus, only at high latitudes (where the QG supercriticality increases above unity) the β term might affect the barotropization. As the β term decreases with latitude, it shows a direct relation to barotropization (as was shown in *Smith and Vallis* [2001]) at high latitudes (blue circles, Figure 2f), which follows $\beta^{1.1\pm0.17}$ (R^2 =0.88). This is different than the inverse relation found in *Held and Larichev* [1996] at high supercriticality. At low latitudes, on the other hand, there is an inverse relation between the β term and barotropization. *Venaille et al.* [2012] suggested that this relation is due to the tendency of large

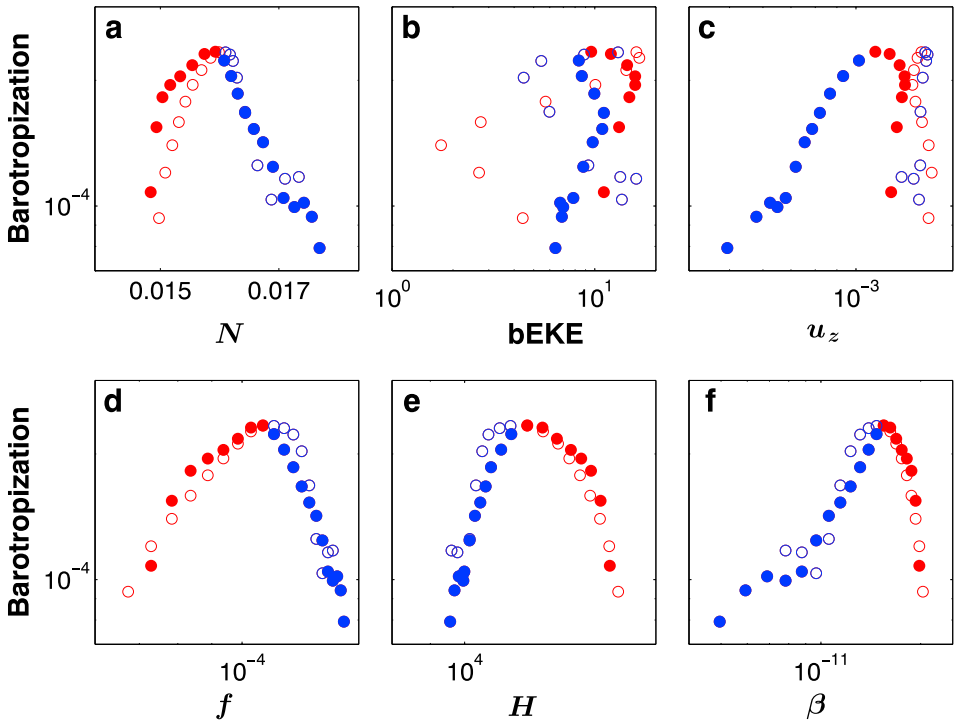

Figure 2. Mean baroclinic to barotropic EKE conversion ($m^2\ s^{-3}$) for different latitudes in the extratropics as a function of (a) mean static stability (N, s^{-1}), (b) barotropic EKE (bEKE, $m^2\ s^{-2}$), (c) vertical shear of the zonal wind (u_z, s^{-1}), (d) Coriolis parameter (f, s^{-1}), (e) tropopause height (H, m), and (f) β term (β, $m^{-1}\ s^{-1}$). Each circle represents a specific latitude. The blue (red) circles correspond to latitudes poleward (equatorward) of the latitude of maximum mean barotropization. The closed (open) circles correspond to the Northern (Southern) Hemisphere.

meridional PV gradient to overcome the layer-wise conservation of eddy PV (section 5), which encourages a depth-independent flow only in a turbulent regime (i.e., where the QG supercriticality is above unity) and a depth-dependent flow in a Rossby wave regime (i.e., where the QG supercriticality is below unity). In summary, at low latitudes, the increase of the barotropization may be explained by the increase and decrease of the Coriolis parameter and the tropopause height, respectively. At high latitudes, on the other hand, the increase of the stratification together with the decrease of the β term may explain the decrease of the barotropization.

According to the Rhines-Salmon two-layer phenomenology, the barotropization of the flow should occur at the Rossby wave number. However, through all latitudes the Rossby wave number (gray line in Figure 1a) is smaller than the conversion wave number (red circles in Figure 3a), which is defined as the wave number of maximum baroclinic-barotropic conversion at each latitude (from Figure 1a). The Rossby wave number is calculated using equation (3), where $\lambda_d = 2\pi L_d$ is the Rossby wavelength, with its corresponding Rossby deformation radius, $L_d = \frac{1}{|f|\pi}\int_0^H N dz$ [*Gill*, 1982; *Chelton et al.*, 1998; *Abernathey and Wortham*, 2015]. Since at these scales baroclinic instability is expected to produce EKE [*Eady*, 1949; *Salmon*, 1978], the most unstable wave number (K_m) is calculated following *Smith* [2007], by preforming a QG linear stability analysis, and compared to the conversion wave number (purple circles, Figure 3b). Different than the Rossby wave number, the most unstable wave number does follow the conversion wave number through all latitudes, especially in the SH. Similar behavior was shown to occur in both atmospheric idealized GCMs [*Jansen and Ferrari*, 2012; *Chemke and Kaspi*, 2015, 2016b] and oceanic state estimates [*Chemke and Kaspi*, 2016a]. Thus, the barotropization of the flow is likely concentrated at midlatitudes since it is coupled to baroclinic instability [*Salmon*, 1978; *Vallis*, 2006], which is mostly important at midlatitudes, and due to the latitudinal dependence of the sphericity parameters, stratification, and tropopause height.

4. Inverse Energy Cascade in the Barotropic Mode

The input of barotropic energy from the baroclinic modes is transferred by advection among different scales. The barotropic eddy-mean flow interactions remove this input of energy and transfer it directly to the zero

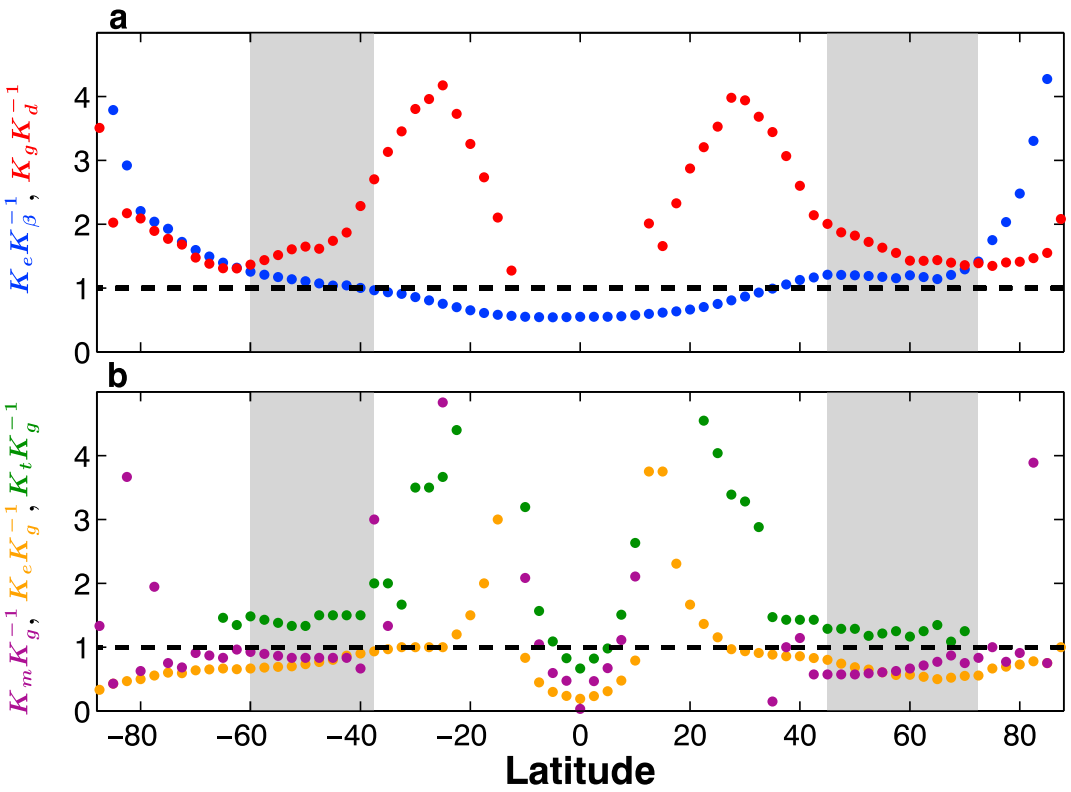

Figure 3. Ratios of macroturbulent wave numbers as a function of latitude. (a) The ratio of the conversion and Rossby wave numbers (red circles) and the ratio of the energy-containing and Rhines wave numbers (blue circles). (b) The ratio of the most unstable and conversion wave numbers (purple circles), the ratio of the energy-containing and conversion wave numbers (orange circles) and the ratio of the transition (see text for definition) and conversion wave numbers (green circles). The shaded areas represent latitudes where an explicit inverse energy cascade occurs according to Figure 1c.

zonal wave number (Figure 1b), which maintains the barotropic zonal mean eddy-driven jets [*Held*, 1975; *Simmons and Hoskins*, 1978]. While in the NH the eddy-mean flow interactions are localized around 25°N, in the SH they are spread at midlatitudes with a maximum around 42°S. Different than the global stratospheric analysis of *Burgess et al.* [2013], here the barotropic eddy-mean flow interactions do not add EKE to other scales beside the zero zonal wave number. Eddy-eddy interactions also play a major role in the balance, but only at high latitudes (Figure 1c), as was also shown in idealized atmospheric GCM simulations [*Chemke and Kaspi*, 2015, 2016b] and oceanic state estimates [*Chemke and Kaspi*, 2016a]. A classic 2-D turbulence picture emerges at these latitudes, where the eddy-eddy interactions spread the input of EKE from the baroclinic modes both upscale and downscale. Similar behavior was shown to occur globally using a 2-D spectra of reanalysis data [*Boer and Shepherd*, 1983; *Shepherd*, 1987; *Straus and Ditlevsen*, 1999; *Burgess et al.*, 2013]. The presence of eddy-eddy interactions at high latitudes may also contribute to the decrease in barotropization at these latitudes [*Chemke and Kaspi*, 2016b].

Barotropic inverse energy cascade occurs when the conversion of baroclinic to barotropic wave number is larger than the energy-containing wave number (K_e, defined at each latitude as the wave number where the spectrum of the barotropic meridional velocity is at maximum) [*O'Gorman and Schneider*, 2008; *Kidston et al.*, 2011; *Chemke and Kaspi*, 2016b]. Indeed, the conversion wave number exceeds the energy-containing wave number (orange circles, Figure 3b) at latitudes, where according to Figure 1c, inverse energy cascade takes place (shaded areas in Figure 3). At higher latitudes, the conversion wave number is still larger than the energy-containing wave number; however, inverse energy cascade is suppressed since the input of energy from the baroclinic modes vanishes (Figure 1a). At lower latitudes in the extratropics these scales almost coincide, which limits the inverse energy cascade. Furthermore, despite the effect of bottom drag on the energy-containing scale [e.g., *Danilov and Gurarie*, 2002; *Smith and Vallis*, 2002; *Thompson and Young*, 2007], the Rhines and energy-containing wave numbers coincide at latitudes of inverse cascade (blue circles,

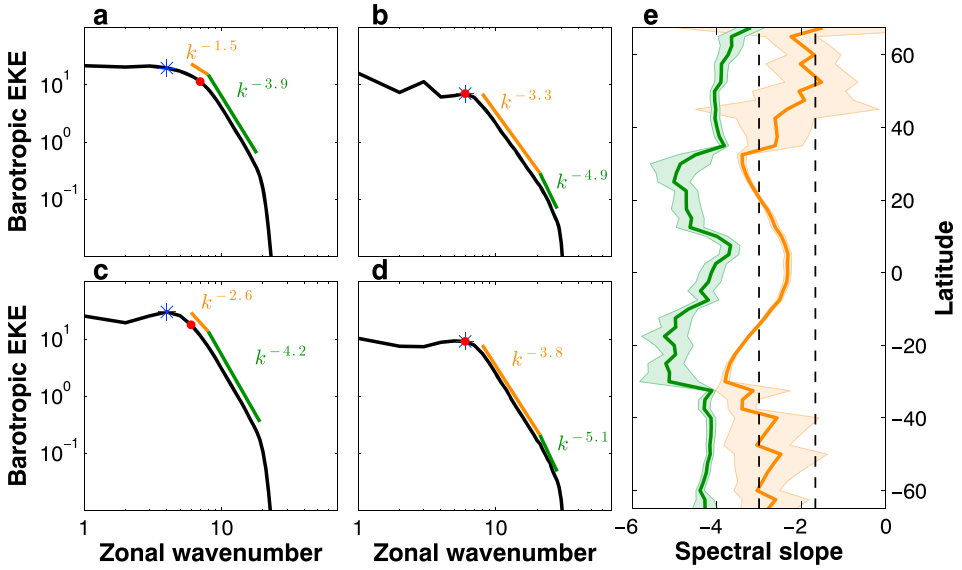

Figure 4. The zonal spectrum of the barotropic EKE ($m^2\ s^{-2}$) as a function of zonal wave number at (a) 52°N, (b) 27°N, (c) 52°S, and (d) 27°S. The blue asterisk and red dot are the energy-containing wave number and conversion wave number of baroclinic to barotropic EKE, respectively. The orange and green lines are the best linear fit slopes. (e) The spectral slopes as function of latitude with shading representing the 95% confidence intervals. The two vertical dashed lines correspond to the −5/3 and −3 slopes.

Figure 3a) as expected from *Rhines* [1975] theory and was shown to occur in both idealized GCM simulations [*Jansen and Ferrari*, 2012; *Chai and Vallis*, 2014; *Chemke and Kaspi*, 2016b] and oceanic state estimates [*Chemke and Kaspi*, 2016a]. This is also evident by the fact that the Rhines wave number follows the inverse energy transfer of eddy-eddy interactions (Figure 1c). The Rhines wave number is calculated using equation (3), where $\lambda_\beta = 2\pi L_\beta$ is the Rhines wavelength and $L_\beta = \left(\frac{\mathrm{EKE}^{0.5}}{\beta}\right)^{0.5}$ is the Rhines scale [*Rhines*, 1975].

As the Rossby and conversion wave numbers do not match, the supercriticality latitudes (purple lines in Figure 1) do not follow latitudes where the Rossby and Rhines wave numbers coincide (the crossing of the gray and black lines in Figure 1). Nonetheless, latitudes where inverse energy cascade is observed are separated by the supercriticality latitudes (Figure 1c), which can explain its occurrence only at high latitudes [*Chemke and Kaspi*, 2015]. This addition of barotropic EKE to large scales only at high latitudes contributes the barotropic nature of the eddy-driven jet.

Despite the pronounced inverse energy cascade in both hemispheres (Figure 1c), the zonal barotropic EKE spectrum (equation (1)) follows a −5/3 slope at large scales only in the NH, while in the SH a steeper slope between −2.5 and −3, as was found globally in *Straus and Ditlevsen* [1999] (orange lines in Figures 4a, 4c, and 4e). However, in both hemispheres the slopes have low statistical significance. The slopes are determined at each latitude through linear least squares fitting of the spectrum in log-log space. The fitting algorithm finds the best fit slopes below the energy-containing wave number and up to the dissipation range, where the spectrum rapidly declines. The lack of a −5/3 slope at large scales might be due to the small-scale separation between the energy-containing (blue asterisks, Figure 4) and conversion (red circles, Figure 4) wave numbers. This reduces the region where the spectrum follows $k^{-5/3}$, which causes the large uncertainty in the slopes' values at high latitudes (Figure 4e). Furthermore, the broad input of baroclinic EKE (Figure 1a) may explain the steeper slopes in the SH at large scales [*Larichev and Held*, 1995].

At low latitudes the upper branch of the spectrum ranges between a slope of −2.5 and −3.8 (orange lines in Figures 4b, 4d, and 4e). In 2-D spectra analysis the tropics contribute more to the resulted spectrum, which might explain why previous reanalysis 2-D spectra studies [e.g., *Boer and Shepherd*, 1983; *Trenberth and Solomon*, 1993; *Burgess et al.*, 2013] showed a similar range of slopes through all heights. A steeper slope than the −3 slope, expected from 2-D turbulence [*Kraichnan*, 1967], is also found at smaller scales at high latitudes, where the spectrum follows a −4 slope (green lines in Figures 4a, 4c, and 4e), which might occur due to the parameterizations of bottom drag and dissipation processes in the reanalysis [*Rivière et al.*, 2004;

Thompson and Young, 2006; *Arbic and Scott*, 2008; *Jansen and Held*, 2014]. Similar to several previous studies [*Boer and Shepherd*, 1983; *Shepherd*, 1987; *Trenberth and Solomon*, 1993; *Straus and Ditlevsen*, 1999], there is no signature of a shallower spectral slope in mesoscales as found by *Nastrom and Gage* [1985] and was shown to occur in both 1-D [*Koshyk and Hamilton*, 2001; *Hamilton et al.*, 2008] and 2-D spectra [*Burgess et al.*, 2013; *Hamilton et al.*, 2008]. This may be explained by the fact that the shallower slope in mesoscales was found to occur mostly in the stratosphere [*Burgess et al.*, 2013], while the barotropic spectrum in Figure 4 includes all heights. Even though the spectral slopes do not show the classic behavior of 2-D turbulence, the transition wave number (K_t), which separates the two slopes at each latitude, implies the existence of two turbulent regimes at smaller and larger wave numbers. The transition wave number is found to follow the conversion wave number mostly at high latitudes, where inverse energy cascade takes place (green circles, Figure 3b). This may indicate that the forward Z and inverse energy cascades at large and small wave numbers, respectively, by eddy-eddy interactions (Figure 1c) are triggered by the barotropization of the flow (Figure 1a).

5. Barotropic Eddy Enstrophy Balance

Similar to the barotropization of EKE, the Z also undergoes barotropization in the extratropics, reaching a maximum value at midlatitudes (Figure 1d). In spite of the layer-wise conservation of QG potential enstrophy in pressure coordinates, the mean meridional PV gradient together with diabatic heating and dissipation terms enable the barotropization of Z mostly poleward of the supercritical latitude [*Venaille et al.*, 2012]. Concomitantly, the eddy-eddy interactions transfer the Z to smaller scales (forward cascade, Figure 1f) as expected from the two-layer baroclinic turbulence phenomenology [*Rhines*, 1977; *Salmon*, 1978]. Forward Z cascade, calculated using the relative vorticity alone, was also shown to occur in 2-D spectra analysis [*Boer and Shepherd*, 1983; *Straus and Ditlevsen*, 1999; *Burgess et al.*, 2013]. Similar to the inverse energy cascade (Figure 1c), forward Z cascade occurs poleward of the supercriticality latitudes, pointing to the importance of the supercriticality in assessing the role of eddy-eddy interactions in the atmosphere. The forward Z cascade latitudinal distribution might be also related to the filamentation of PV in critical latitudes [*Thorncroft et al.*, 1993].

Most of the barotropic Z transfers occur from the mean flow to the eddies (Figure 1e). The dominant term in equation (8), which is responsible for most of this Z transfer, is $-[v]'[q]'\frac{\partial[q]}{a\partial\vartheta}$ (Figure 1e). This term contributes to the growth of waves (increases Z) as it is everywhere positive [*Held*, 1975; *Held and Hoskins*, 1985]. As the meridional gradient of the QGPV is everywhere positive, the meridional flux, $[v]'[q]'$, must be everywhere negative (downgradient), and this may occur if it is diffusive [*Green*, 1970; *Held and Larichev*, 1996]. In the Rhines-Salmon phenomenology, the eddy-mean flow interactions do not play a major role in the balance as the Coriolis parameter and static stability were taken as constants (i.e., small meridional QGPV gradient). Repeating the calculations of the Z transfers (equations (7)–(9)) for the QGPV only with constant f and S^2 shows a similar picture to the classic two-layer phenomenology, where the main balance of Z in the barotropic mode is between the barotropization and the forward Z cascade (Figures 1g–1i). Thus, in Earth's atmosphere, the significant meridional QGPV gradient strengthens the role of eddy-mean flow interactions in adding Z to the eddies, at the expense of the baroclinic-barotropic transfer.

Acknowledgments
We thank Isaac Held and Ted Shepherd for helpful conversations. We also thank Antoine Venaille and an anonymous reviewer whose comments have helped to improve the manuscript. This research has been supported by the Israeli Science Foundation (grant 1310/12), the Israeli Ministry of Science, and the Minerva foundation with funding from the Federal German Ministry of Education and Research.

References

Abernathey, R., and C. Wortham (2015), Phase speed cross spectra of eddy heat fluxes in the eastern Pacific, *J. Phys. Oceanogr.*, *45*, 1285–1301.

Arbic, B. K., and G. R. Flierl (2004), Baroclinically unstable geostrophic turbulence in the limits of strong and weak bottom Ekman friction: Application to midocean eddies, *J. Phys. Oceanogr.*, *34*, 2257–2273.

Arbic, B. K., and R. B. Scott (2008), On quadratic bottom drag, geostrophic turbulence, and oceanic mesoscale eddies, *J. Phys. Oceanogr.*, *38*, 84–103.

Boer, G. J., and T. G. Shepherd (1983), Large-scale two-dimensional turbulence in the atmosphere, *J. Atmos. Sci.*, *40*(1), 164–184.

Burgess, B. H., A. R. Erler, and T. G. Shepherd (2013), The troposphere-to-stratosphere transition in kinetic energy spectra and nonlinear spectral fluxes as seen in ECMWF analyses, *J. Atmos. Sci.*, *70*, 669–687.

Chai, J., and G. K. Vallis (2014), The role of criticality on the horizontal and vertical scales of extratropical eddies in a dry GCM, *J. Atmos. Sci.*, *71*(7), 2300–2318.

Charney, J. G. (1971), Geostrophic turbulence, *J. Atmos. Sci.*, *28*(6), 1087–1095.

Charney, J. G., and M. E. Stern (1962), On the stability of internal baroclinic jets in a rotating atmosphere, *J. Atmos. Sci.*, *19*(2), 159–172.

Chelton, D. B., R. A. Deszoeke, M. G. Schlax, E. Naggar, and N. Siwertz (1998), Geographical variability of the first baroclinic Rossby radius of deformation, *J. Phys. Oceanogr.*, *28*(3), 433–460.

Chemke, R., and Y. Kaspi (2015), The latitudinal dependence of atmospheric jet scales and macroturbulent energy cascades, *J. Atmos. Sci.*, *72*(10), 3891–3907.
Chemke, R., and Y. Kaspi (2016a), The latitudinal dependence of the oceanic barotropic eddy kinetic energy and macroturbulence energy transport, *Geophys. Res. Lett.*, *43*, 2723–2731, doi:10.1002/2016GL067847.
Chemke, R., and Y. Kaspi (2016b), The effect of eddy-eddy interactions on jet formation and macroturbulent scales, *J. Atmos. Sci.*, *73*(5), 2049–2059.
Danilov, S., and D. Gurarie (2002), Rhines scale and spectra of the beta plane turbulence with bottom drag, *Phys. Rev. E*, *65*(6), 67301.
Dee, D. P., et al. (2011), The ERA-Interim reanalysis: Configuration and performance of the data assimilation system, *Q. J. R. Meteorol. Soc.*, *137*, 553–597.
Eady, E. T. (1949), Long waves and cyclone waves, *Tellus*, *1*(3), 33–52.
Edmon, J. H. J., B. J. Hoskins, and M. E. McIntyre (1980), Eliassen-Palm cross sections for the troposphere, *J. Atmos. Sci.*, *37*(12), 2600–2612.
Fu, L.-L., and G. R. Flierl (1980), Nonlinear energy and enstrophy transfers in a realistically stratified ocean, *Dyn. Atmos. Oceans*, *4*(4), 219–246.
Gill, A. E. (1982), *Atmosphere-Ocean Dynamics*, 662 pp., Academic Press, San Diego, Calif.
Green, J. S. A. (1970), Transfer properties of the large-scale eddies and the general circulation of the atmosphere, *Q. J. R. Meteorol. Soc.*, *96*(408), 157–185.
Hamilton, K., Y. O. Takahashi, and W. Ohfuchi (2008), Mesoscale spectrum of atmospheric motions investigated in a very fine resolution global general circulation model, *J. Geophys. Res.*, *113*, D18110, doi:10.1029/2008JD009785.
Held, I. M. (1975), Momentum transport by quasi-geostrophic eddies, *J. Atmos. Sci.*, *32*, 1494–1496.
Held, I. M., and B. J. Hoskins (1985), Large-scale eddies and the general circulation of the troposphere, *Adv. Geophys.*, *28*, 3–31.
Held, I. M., and V. D. Larichev (1996), A scaling theory for horizontally homogeneous, baroclinically unstable flow on a beta plane, *J. Atmos. Sci.*, *53*(7), 946–952.
Hoskins, B. J., M. E. McIntyre, and A. W. Robertson (1985), On the use and significance of isentropic potential vorticity maps, *Q. J. R. Meteorol. Soc.*, *111*, 877–946.
Jansen, M., and R. Ferrari (2012), Macroturbulent equilibration in a thermally forced primitive equation system, *J. Atmos. Sci.*, *69*(2), 695–713.
Jansen, M. F., and I. M. Held (2014), Parameterizing subgrid-scale eddy effects using energetically consistent backscatter, *Ocean Model.*, *80*, 36–48.
Kanamitsu, M., W. Ebisuzaki, J. Woollen, S.-K. Yang, J. J. Hnilo, M. Fiorino, and G. L. Potter (2002), NCEP-DOE AMIP-II Reanalysis (R-2), *Bull. Am. Meteorol. Soc.*, *83*, 1631–1643.
Kidston, J., G. K. Vallis, S. M. Dean, and J. A. Renwick (2011), Can the increase in the eddy length scale under global warming cause the poleward shift of the jet streams?, *J. Clim.*, *24*(14), 3764–3780.
Koshyk, J. N., and K. Hamilton (2001), The horizontal kinetic energy spectrum and spectral budget simulated by a high-resolution troposphere-stratosphere-mesosphere GCM, *J. Atmos. Sci.*, *58*(4), 329–348.
Koshyk, J. N., B. A. Boville, K. Hamilton, E. Manzini, and K. Shibata (1999), Kinetic energy spectrum of horizontal motions in middle-atmosphere models, *J. Geophys. Res.*, *104*, 27,177–27,190.
Kraichnan, R. H. (1967), Inertial ranges in two-dimensional turbulence, *Phys. Fluids*, *10*, 1417–1423.
Larichev, V. D., and I. M. Held (1995), Eddy amplitudes and fluxes in a homogeneous model of fully developed baroclinic instability, *J. Phys. Oceanogr.*, *25*(10), 2285–2297.
Lee, S., and H. Kim (2003), The dynamical relationship between subtropical and eddy-driven jets, *J. Atmos. Sci.*, *60*, 1490–1503.
Nastrom, G. D., and K. A. Gage (1985), A climatology of atmospheric wavenumber spectra of wind and temperature observed by commercial aircraft, *J. Atmos. Sci.*, *42*(9), 950–960.
O'Gorman, P. A., and T. Schneider (2008), Weather-layer dynamics of baroclinic eddies and multiple jets in an idealized general circulation model, *J. Atmos. Sci.*, *65*(2), 524–535.
Rhines, P. B. (1975), Waves and turbulence on a beta plane, *J. Fluid Mech.*, *69*(03), 417–443.
Rhines, P. B. (1977), The dynamics of unsteady currents, *The Sea*, *6*, 189–318.
Rivière, P., A. M. Treguier, and P. Klein (2004), Effects of bottom friction on nonlinear equilibration of an oceanic baroclinic jet, *J. Phys. Oceanogr.*, *34*, 416–432.
Salmon, R. (1978), Two-layer quasi-geostrophic turbulence in a simple special case, *Geophys. Astrophys. Fluid Dyn.*, *10*(1), 25–52.
Saltzman, B. (1957), Equations governing the energetics of the larger scales of atmospheric turbulence in the domain of wave number, *J. Meteorol.*, *14*(6), 513–523.
Schlösser, F., and C. Eden (2007), Diagnosing the energy cascade in a model of the North Atlantic, *Geophys. Res. Lett.*, *34*, L02604, doi:10.1029/2006GL027813.
Schneider, T. (2006), The general circulation of the atmosphere, *Ann. Rev. Earth Planet. Sci.*, *34*, 655–688.
Scott, R. B., and B. K. Arbic (2007), Spectral energy fluxes in geostrophic turbulence: Implications for ocean energetics, *J. Phys. Oceanogr.*, *37*(3), 673–688.
Scott, R. B., and F. Wang (2005), Direct evidence of an oceanic inverse kinetic energy cascade from satellite altimetry, *J. Phys. Oceanogr.*, *35*(9), 1650–1666.
Shepherd, T. G. (1987), A spectral view of nonlinear fluxes and stationary-transient interaction in the atmosphere, *J. Atmos. Sci.*, *44*(8), 1166–1147.
Simmons, A. J., and B. J. Hoskins (1978), The life cycles of some nonlinear baroclinic waves, *J. Atmos. Sci.*, *35*(3), 414–432.
Smith, K. S. (2007), The geography of linear baroclinic instability in Earth's oceans, *J. Mar. Res.*, *65*(5), 655–683.
Smith, K. S., and G. K. Vallis (2001), The scales and equilibration of midocean eddies: Freely evolving flow, *J. Phys. Oceanogr.*, *31*(2), 554–571.
Smith, K. S., and G. K. Vallis (2002), The scales and equilibration of midocean eddies: Forced-dissipative flow, *J. Phys. Oceanogr.*, *32*(6), 1699–1720.
Straus, D. M., and P. Ditlevsen (1999), Two-dimensional turbulence properties of the ECMWF reanalyses, *Tellus A*, *51*, 749–772.
Thompson, A. F., and W. R. Young (2006), Scaling baroclinic eddy fluxes: Vortices and energy balance, *J. Phys. Oceanogr.*, *36*, 720–738.
Thompson, A. F., and W. R. Young (2007), Two-layer baroclinic eddy heat fluxes: Zonal flows and energy balance, *J. Phys. Oceanogr.*, *64*, 3214–3231.
Thorncroft, C. D., B. J. Hoskins, and M. E. McIntyre (1993), Two paradigms of baroclinic-wave life-cycle behaviour, *Q. J. R. Meteorol. Soc.*, *119*, 17–55.
Treguier, A. M., and B. L. Hua (1988), Influence of bottom topography on stratified quasi-geostrophic turbulence in the ocean, *Geophys. Astrophys. Fluid Dyn.*, *43*, 265–305.

Trenberth, K. E., and A. Solomon (1993), Implications of global atmospheric spatial spectra for processing and displaying data., *J. Clim.*, *6*, 531–545.

Vallis, G. K. (2006), *Atmospheric and Oceanic Fluid Dynamics*, Cambridge Univ. Press, 770 pp., Cambridge, U. K.

Venaille, A., G. K. Vallis, and S. M. Griffies (2012), The catalytic role of the beta effect in barotropization processes, *J. Fluid Mech.*, *709*, 490–515.